Data-driven linear parameter-varying modelling of the steering dynamics of an autonomous car

G. Rödönyi *,**, **R. Tóth** **,***, **D. Pup** *, **Á. Kisari** *,**,
Zs. Vígh **, **P. Kőrös** *, **J. Bokor** **

* Research Center of Vehicle Industry, Széchenyi István University,
Egyetem tér 1, H-9026 Győr, Hungary. (email: rodonyi@sztaki.hu)
** Systems and Control Laboratory, Institute for Computer Science and
Control, Kende u. 13-17, H-1111 Budapest, Hungary.
*** Control Systems Group, Eindhoven University of Technology, P.O.
Box 513, 5600 MB Eindhoven, The Netherlands.

Abstract: Developing automatic driving solutions and driver support systems requires accurate vehicle specific models to describe and predict the associated motion dynamics of the vehicle. Despite of the mature understanding of ideal vehicle dynamics, which are inherently nonlinear, modern cars are equipped with a wide array of digital and mechatronic components that are difficult to model. Furthermore, due to manufacturing, each car has its personal motion characteristics which change over time. Hence, it is important to develop data-driven modelling methods that are capable to capture from data all relevant aspects of vehicle dynamics in a model that is directly utilisable for control. In this paper, we show how Linear Parameter-Varying (LPV) modelling and system identification can be applied to reliably capture personalised model of the steering system of an autonomous car based on measured data. Compared to other nonlinear identification techniques, the obtained LPV model is directly utilisable for powerful controller synthesis methods of the LPV framework.

Keywords: Vehicle dynamics; system identification; linear parameter-varying systems.

1. INTRODUCTION

The spreading of autonomous vehicles in transportation and traffic promises to bring benefits in terms of higher level of safety, energy efficiency, reduced emission and congestion, see Anderson et al. (2014). However, most modern road vehicles are complex nonlinear dynamic systems with digitally driven mechatronic components and with behavior that is strongly influenced by environmental conditions. Therefore, accurate vehicle modeling and complete control of the motion dynamics are challenging problems. The dominant modeling paradigm is to build first principle models based on physical equations (Berntorp et al. (2014); Kiencke and Nielsen (2000)). Physical parameters can often be estimated on the fly and utilized in an adaptive control setting (Singh and Taheri (2015)). This approach allows comforting insight and thereby confidence in the model. Depending on the purpose of application and the assumed environmental conditions, physical models of different complexity have been developed, see Althoff et al. (2017) for some examples. However, these mechanistic models are based on ideal vehicle characteristics and often fail to express relevant dynamic effects in a specific vehicle that are beyond the ideal motion dynamics.

An alternative way is to apply data-driven modeling methods in terms of system identification. In the past decades,

system identification, especially for *linear time-invariant* (LTI) systems, became a mature framework with powerful methods from experiment design to model estimation, providing statistical guarantees in terms of consistency and characterization of uncertainty of the estimated models (Ljung, 1999). However, identification of nonlinear systems, such as the vehicle dynamics, is still under development. Recent nonlinear identification methods supported by machine learning are promising, offering flexible model structures to capture the system behavior (Schoukens and Ljung, 2019), but the obtained models are often too complex for control and nonlinear control methods often lack performance shaping capabilities. The framework of *linear parameter-varying* (LPV) systems has appeared as a paradigm to bring the two worlds together, offering model structures that can describe nonlinear systems in terms of a linear dynamic relation which is dependent on a measurable scheduling variable (Tóth, 2010). Linearity of these representations allowed the extension of the powerful control synthesis methods to achieve performance shaping and stabilization of nonlinear systems (Hoffmann and Werner, 2015; Hjartarson et al., 2015). It has been already shown that LPV modeling and control is attractive for motion control of vehicles (Poussot-Vassal et al., 2013). Also recently, system identification of LPV systems has matured, offering a wide range of tools to estimate LPV models directly applicable in control synthesis, see the overviews in (Tóth (2010); Cox and Tóth (2021)) and the references therein.

In this paper we are interested in developing a model for controlling the lateral dynamics of a Nissan Leaf test vehicle which serves as a platform for autonomous driving research. As a steering actuator, the built-in *electric power steering* (EPS) system is utilized. In normal operation, the EPS receives a voltage signal proportional to the measured steering-wheel torque applied by the driver. With a minimal-cost hardware modification, this connection is augmented: the autonomous vehicle controller running on an external computer produces an additional voltage input to the servo system. This concept worked well with a base-line controller as demonstrated in Szűcs et al. (2020), but a more accurate model-based controller is required to increase performance and reduce the strain to the servo.

Lateral vehicle dynamic models are frequently applied for performance analysis and synthesis of steering controllers, (Berntorp et al. (2014)), where the control input is the steering angle of the front wheels and the measurable outputs are the yaw-rate and the lateral acceleration. A typical challenge in modeling and control occurs under extreme driving conditions, when the nonlinear and road-surface dependent tire adhesion characteristics play a significant role. The Nissan Leaf test vehicle challenges model identification even in normal driving conditions: 1.) accurate structural information or a model of the EPS system, used as control actuator, are rarely disclosed by any manufacturer; 2.) there is a nonlinear feedback from the lateral tire forces to the steering linkages through the steering angle dependent self-aligning force arm which is highly influenced by the actual undercarriage settings; 3.) in addition to the above unknown nonlinear effects, the steering system being a weakly damped subsystem is sensitive to disturbances that makes the modeling of a nonlinear system particularly hard. This challenging modeling problem has been successfully solved with learning-based tools, such as Gaussian processes and neural networks, Rödönyi et al. (2021), but much lower order, simpler models are required for control design that can still adequately express the challenging nonlinear dynamics.

Inspired by the attractive properties of data-driven LPV modeling and developing software toolboxes, such as LPV-core (den Boef et al. (2021)), in this paper we study black-box LPV identification of the motion dynamics associated with the EPS-actuated test vehicle in terms of *prediction error methods* (PEM) to study how well such models are capable to recover the nonlinear dynamics and explain the effect of disturbances. To provide a detailed analysis of the estimation process and reliable characterization of the archived performance, we develop a high-fidelity simulation environment of the steering dynamics. This data generating simulator model contains all known structural information and its parameters are tuned to fit the dominant behavior of the true Nissan Leaf. In our study, we demonstrate that LPV-PEM methods can successfully recover the system dynamics under realistic noise and disturbance conditions.

The paper is structured as follows: in Section 2, we develop a high-fidelity simulator model of the steering dynamics of the Nissan Leaf test vehicle. Then, in Section 3, a single-track approximation and LPV embedding of the high-fidelity continuous-time model is developed. After describing the used black-box discrete-time LPV-PEM identifica-
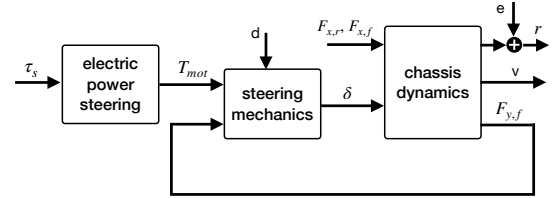

Fig. 1. Sub-components of the system describing the steering dynamics. Measurement data for τ_s, δ, r and v are available for identification.

tion concept in Section 4, the experiment design and model estimation of the steering dynamics are analyzed in terms of both the embedding based physical LPV model and the black-box PEM. Conclusions on the established results and perspectives of future research are given in Section 7.

2. FIRST PRINCIPLES-BASED MODELING

In this section, based on known physical relations, we develop a high-fidelity model of the steering dynamics of the Nissan Leaf which will be used for our simulator.

2.1 Overview

The system to be modeled can be divided into three main parts depicted in Fig. 1: the electric power steering unit, the steering mechanics, and the vehicle chassis dynamics. The input signals and the state variables together with the relevant parameters associated with the representation of the system dynamics are summarized in Tables 1-3. Steering of the Nissan Leaf electric test vehicle is controlled by the EPS unit. During autonomous operation, the driver releases the steering-wheel and an input voltage signal τ_s is generated by the on-board computer. This input is processed by the EPS system to produce a torque on the steering column. A second, self-aligning torque due to the tire-road contact also acts on the steering linkages. The EPS system and the steering mechanics are modeled in Section 2.3. The state of the steering system is represented by the steering angle, δ, which is also an input to the chassis dynamics described in Section 2.2.

2.2 Lateral Chassis Dynamics

The lateral chassis dynamics is well-studied and models are available from the simplest kinematic and bicycle-type models to the high dimensional multi-body descriptions

Table 1. Input signals of the simulation model.

Definition	Notation	Unit
Control input (requested steering torque)	τ_s	V
Driving/braking force at the front	$F_{x,f}$	N
Driving/braking force at the rear	$F_{x,r}$	N
Disturbance at the steering system	d	rad/s
Yaw-rate sensor noise	e	rad/s

Table 2. State variables of the model.

Definition	Notation	Unit
Longitudinal speed	v_x	m/s
Lateral speed	v_y	m/s
Yaw rate	r	rad/s
Pitch angle	θ	rad
Pitch rate	$\dot{\theta}$	rad/s
Roll angle	ϕ	rad
Roll rate	$\dot{\phi}$	rad/s
Wheel slip angle	$\alpha_i, \quad i = 1, 2, 3, 4$	rad
Steering angle	δ	rad

Table 3. Parameters of the simulation model.

Definition	Notation	Value	Unit
wheelbase	$l = l_r + l_f$	2.7	m
track	w	0.77	m
vehicle mass	m	1860	kg
gravity constant	g	9.81	m/s^2
front axle-CG dist.	l_f	1.65	m
rear axle-CG dist.	l_r	1.05	m
pitch inertia	I_{xx}	737.8	kgm^2
roll inertia	I_{yy}	2840	kgm^2
yaw inertia	I_{zz}	2925	kgm^2
height of COG	h	0.623	m
lateral slip time const.	σ	0.375	m
roll stiffness	K_ϕ	66751	Nm/rad
roll damping	D_ϕ	6260	Nms/rad
pitch stiffness	K_θ	408500	Nm/rad
pitch damping	D_θ	35269	Nms/rad
cornering stiffness coeff.	$c_1 = c_2$	8.5	1/rad
cornering stiffness coeff.	$c_3 = c_4$	11.5	1/rad
boost map coefficient	A	0.0063	-
boost map coefficient	a	8.677	1/Nm
boost map coefficient	b	0	s/m
steering mech. coeff.	a_δ	0.108	1/s
steering mech. coeff.	b_b	2.369	rad/Nms
steering mech. coeff.	b_l	2.546	rad/Nms
self-aligning force-arm	$n(\delta)$	see (9)	m

Berntorp (2013); Kiencke and Nielsen (2000); Bertolazzi et al. (2007). For testing control oriented LPV model identification methods, a medium complexity *double-track* (DT) nonlinear model is chosen. The chassis model has two translational and three rotational degrees of freedom. The suspension system is modeled as a rotational spring-damper system where roll and pitch motions are responsible for load transfer at the wheels. To develop a model for normal driving conditions and small tire slips, wheel dynamics and nonlinear tire adhesion characteristic are neglected. The equations are derived based on Berntorp (2013) using also the wheel speed kinematics from Kiencke and Nielsen (2000). Wheels are indexed as follows: 1-front left, 2-front right, 3-rear left, 4-rear right. The vertical load $F_z = [F_{z,1} \; F_{z,2} \; F_{z,3} \; F_{z,4}]^\top$ at the tire-road contact points varies due to the pitch (θ) and roll (ϕ) motion of the chassis

$$F_z = \frac{mg}{2l}\begin{bmatrix} l_r \\ l_r \\ l_f \\ l_f \end{bmatrix} + \frac{1}{2lw}\begin{bmatrix} w & -l \\ w & l \\ -w & -l \\ -w & l \end{bmatrix}\begin{bmatrix} K_\theta\theta + D_\theta\dot\theta \\ K_\phi\phi + D_\phi\dot\phi \end{bmatrix}, \quad (1)$$

where l_f, l_r, l and w are geometric parameters. Wheel loads affect the lateral tire forces $F_{y,i}$. Regarding the tire model, we assume small acceleration/deceleration and thereby small longitudinal wheel slip. At the range of small slips, the lateral tire force can be well approximated as the product of the lateral wheel slip angle α_i, and the cornering stiffness, $c_{\alpha,i} = c_i F_{z,i}$, where the cornering stiffness coefficients c_i involve the effects of adhesion coefficients. So the lateral forces perpendicular to the wheel plains can be expressed as $\{F_{y,i} = c_i F_{z,i}\alpha_i\}_{i=1}^4$. In steady-state cornering, wheel side-slip angles α_i can be defined as the angle between the wheel plain and the speed vector $v_{w,i}$ of the wheel centre with

$$\dot\alpha_i = \frac{1}{\sigma}\left(-\alpha_i - \tan^{-1}\left(\frac{v_{wy,i}}{v_{wx,i}}\right)\right)v_{wx,i}, \quad i \in \{1,\dots,4\}, \quad (2)$$

where σ is a time-constant. The components $v_{w,x,i}$ and $v_{w,y,i}$ of the wheel centre speed defined in the wheel coordinate frames can be calculated from the rigid body

motion of the vehicle via the yaw-rate and the speed vector $[v_x \; v_y]^\top$ of the mass centre

$$v_{wx} = \begin{bmatrix} \cos(\delta)(v_x - rw) + \sin(\delta)(v_y + rl_f) \\ \cos(\delta)(v_x + rw) + \sin(\delta)(v_y + rl_f) \\ v_x - rw \\ v_x + rw \end{bmatrix}, \quad (3a)$$

$$v_{wy} = \begin{bmatrix} -\sin(\delta)(v_x - rw) + \cos(\delta)(v_y + rl_f) \\ -\sin(\delta)(v_x + rw) + \cos(\delta)(v_y + rl_f) \\ v_y - rl_r \\ v_y - rl_r \end{bmatrix}. \quad (3b)$$

The global external forces and yaw moment acting on the vehicle body can be calculated by summing up the lateral and longitudinal tire force components as follows

$$F_X = F_{x,f}\cos(\delta) - F_{y,f}\sin(\delta) + F_{x,r} \quad (4a)$$

$$F_Y = F_{x,f}\sin(\delta) + F_{y,f}\cos(\delta) + F_{y,r} \quad (4b)$$

$$M_Z = l_f\left(F_{x,f}\sin(\delta) + F_{y,f}\cos(\delta)\right) - l_r F_{y,r} + w\,(F_{x,4} \quad (4c)$$
$$- F_{x,3} + (F_{x,2} - F_{x,1})\cos(\delta) + (F_{y,1} - F_{y,2})\sin(\delta))$$

with shorthand notations: $F_{x,f} = F_{x,1} + F_{x,2}$, $F_{x,r} = F_{x,3} + F_{x,4}$, $F_{y,f} = F_{y,1} + F_{y,2}$, $F_{y,r} = F_{y,3} + F_{y,4}$.

The translational and rotational dynamic equations of the chassis are derived based on the Newton-Euler approach

$$\dot v_x = v_y r + \frac{1}{m}F_X$$
$$+ h\left(\cos(\phi)(\sin(\theta)(r^2 + \dot\phi^2 + \dot\theta^2) - 2\dot\phi r - \cos(\theta)\ddot\theta)\right.$$
$$\left. + \sin(\phi)(2\cos(\theta)\dot\theta\dot\phi + \sin(\theta)\ddot\phi - \dot r)\right), \quad (5a)$$

$$\dot v_y = -v_x r + \frac{1}{m}F_Y + h\left(\cos(\phi)(-\sin(\theta)\dot r - 2\cos(\theta)\dot\theta r + \ddot\phi)\right.$$
$$\left. + \sin(\phi)(\sin(\theta)\dot\phi r - \dot\phi^2 - r^2)\right), \quad (5b)$$

$$\dot r = \frac{M_Z - h(F_X\sin(\phi) + F_Y\sin(\theta)\cos(\phi))}{I_{xx}\sin^2(\theta) + \cos^2(\theta)(I_{yy}\sin^2(\phi) + I_{zz}\cos^2(\phi))}, \quad (5c)$$

$$\Omega_y\ddot\theta = rC_{\theta,r} - (K_\theta\theta + D_\theta\dot\theta)$$
$$+ h(mg\sin(\theta) - F_X\cos(\theta))\cos(\phi), \quad (5d)$$

$$\Omega_x\ddot\phi = -2(K_\phi\phi + D_\phi\dot\phi) + h\left(F_Y\cos(\phi)\cos(\theta) + mg\sin(\phi)\right)$$
$$+ (I_{yy} - I_{zz})r\sin(\phi)\cos(\phi)\left(r\cos(\theta) + \dot\phi\sin(\theta)\right)$$
$$+ r\dot\theta(\cos^2(\phi)I_{yy} + \sin^2(\phi)I_{zz}), \quad (5e)$$

where

$$\Omega_x = I_{xx}\cos^2(\theta) + \sin^2(\theta)(I_{yy}\sin^2(\phi) + I_{zz}\cos^2(\phi)) \quad (5f)$$

$$\Omega_y = I_{yy}\cos^2(\phi) + I_{zz}\sin^2(\phi) \quad (5g)$$

$$C_{\theta,r} = r\sin(\theta)\cos(\theta)\left(I_{xx} - I_{yy} + \cos^2(\phi)(I_{yy} - I_{zz})\right)$$
$$- \dot\phi\left(\cos^2(\theta)I_{xx} + \sin^2(\theta)(\sin^2(\phi)I_{yy} + \cos^2(\phi)I_{zz})\right)$$
$$- \dot\theta\sin(\theta)\sin(\phi)\cos(\phi)(I_{yy} - I_{zz}). \quad (5h)$$

Equations (1)-(5h) describe the "chassis dynamics" block in Figure 1.

2.3 Steering Actuation Based on EPS

The steering system is manipulated through the *requested steering torque* τ_s. This torque is affected by a speed dependent boost map

$$\tau_b(\tau_s, v) = \text{sign}(\tau_s)\min(1, A\left(e^{a|\tau_s|(1-bv)} - 1\right). \quad (6)$$

where A, a, b are parameters. The resulting τ_b is passed through a lead-lag compensator and realzied by the electric assist motor that generates torque T_{mot} on the steering column. An other torque that acts on the steering system

is τ_l, called self-aligning torque. It is proportional to the lateral tire forces $F_{y,f}$ through a steering angle dependent force arm coefficient denoted by $n(\delta)$:

$$\tau_l = n(\delta) F_{y,f}. \qquad (7)$$

These torques drive the steering angle through an LTI relation which, under normal driving conditions, can be approximated by a low order filter:

$$\dot{\delta} = -a_\delta \delta + b_b \tau_b + b_l \tau_l + d, \qquad (8)$$

where d represents additional disturbance effects acting on the steering column, a_δ, b_b and b_l are coefficients that are identified from dedicated experiments. The coefficient $n(\delta)$ depends on the wheel settings and therefore varies in general with the steering angle. It is normalized and defined in the simulator model as

$$n(\delta) = \begin{cases} 1 - c_{\text{low}}(\delta_{\text{low}} - \delta)^2 & \text{if } \delta < \delta_{\text{low}} \\ 1 - c_{\text{high}}(\delta_{\text{high}} - \delta)^2 & \text{if } \delta > \delta_{\text{high}} \\ 1 & \text{otherwise} \end{cases} \qquad (9)$$

where $c_{\text{low}} = c_{\text{high}} = 5.2$ and $-\delta_{\text{low}} = \delta_{\text{high}} = 5\frac{\pi}{180}$rad. The quadratic function emulates the experienced effect on the test vehicle that for larger steering angles the assist torque required to maintain a steady cornering decreased and the system became sensitive to disturbing effects. The resulting Eq. (6)-(9) describe both the "electric power steering" and "steering mechanics" blocks in Figure 1.

Discrete implementation of the overall model is achieved via 4$^{\text{th}}$-order *Runge-Kutta* (RK) (using frozen input values in the increments) with step size $T_s = 0.1$s. Measurement of the yaw-rate r is assumed to be effected by an independent discrete-time white noise process e with $e(k) \sim N(0, 0.025^2)$ which represents approximately $\pm 10\%$ amplitude variation of the measurement. Furthermore, the disturbance d in (8) is modeled as a band limited discrete-time noise process with $d_k \sim \mathcal{N}_{[0,\,2.5\text{Hz}]}(0, 0.1^2)$. The resulting overall *signal-to-noise ratio* (SNR) is 12 dB which corresponds to harsh noise conditions.

3. LPV MODEL CONVERSION

Next, we develop a simple LPV model of the system based on approximation and embedding of the nonlinear behavior. This model will be the source of selecting the scheduling variables and used for comparison with the identified LPV models later on.

3.1 Derivation of LPV Single-Track Model

By linearization around the origin of the state-space of the chassis dynamics and neglecting the roll and pitch motion, the right and left sides of the chassis body can be lumped together leading to the *single-track* (ST) chassis model. The single-track chassis model describes the dominant characteristics of the translational and yaw dynamics of the vehicle at normal driving conditions Berntorp et al. (2014). By introducing the state transformation

$$\left. \begin{aligned} \beta &= \tan^{-1}\left(\frac{v_y}{v_x}\right) \\ v &= \sqrt{v_x^2 + v_y^2} \end{aligned} \right\} \Rightarrow \begin{aligned} v_x &\approx v \\ v_y &\approx \beta v \end{aligned} \qquad (10)$$

and neglecting the effect of $F_{x,i}$ on the lateral dynamics, the lateral tire forces at the front and rear axis reduce to

$$F_{y,f}(\alpha_f) = c_f \alpha_f, \quad F_{y,r}(\alpha_r) = c_r \alpha_r \qquad (11)$$

where $c_f = c_1 mgl_r/l$, $c_r = c_3 mgl_f/l$, denote the front and rear cornering stiffness. Longitudinal and lateral components of the speed of the front and real wheel centers are

$$v_{wx} = \begin{bmatrix} v_{wx,f} \\ v_{wx,r} \end{bmatrix} = \begin{bmatrix} v \\ v \end{bmatrix}, \qquad (12)$$

$$v_{wy} = \begin{bmatrix} v_{wy,f} \\ v_{wy,r} \end{bmatrix} = \begin{bmatrix} -\delta v + v\beta + rl_f \\ v\beta - rl_r \end{bmatrix}. \qquad (13)$$

The wheel side-slip angles evolve according to

$$\dot{\alpha}_f = -\frac{v}{\sigma}\alpha_f - \frac{v}{\sigma}\beta - \frac{l_f}{\sigma}r + \frac{v}{\sigma}\delta, \qquad (14)$$

$$\dot{\alpha}_r = -\frac{v}{\sigma}\alpha_r - \frac{v}{\sigma}\beta + \frac{l_r}{\sigma}r. \qquad (15)$$

The global lateral force and yaw moment become

$$F_Y = F_{y,f} + F_{y,r} = c_f \alpha_f + c_r \alpha_r, \qquad (16)$$

$$M_Z = l_f F_{y,f} - l_r F_{y,r} = l_f c_f \alpha_f - l_r c_r \alpha_r. \qquad (17)$$

By using $\dot{v}_y = \dot{\beta}v + \beta\dot{v} = -vr + \frac{c_f}{m}\alpha_f + \frac{c_r}{m}\alpha_r$, the above formulas results in the lateral chassis dynamics

$$\dot{\beta} = -\beta\frac{\dot{v}}{v} - r + \frac{c_f}{mv}\alpha_f + \frac{c_r}{mv}\alpha_r, \qquad (18)$$

$$\dot{r} = \frac{M_Z}{I_{zz}} = \frac{l_f c_f}{I_{zz}}\alpha_f - \frac{l_r c_r}{I_{zz}}\alpha_r. \qquad (19)$$

Finally, the above chassis model is augmented by the steering system model described in Section 2.3. In summary, the overall system is simplified in the following state-space form, which will be referred as the LPV-ST model,

$$\dot{x}_{st} = A(p)x_{st} + B_b\tau_b(\tau_s, v), \qquad (20)$$

with $x_{st} = [\begin{matrix} \beta & r & \alpha_f & \alpha_r & \delta \end{matrix}]^\top$, scheduling $p = [\begin{matrix} v & \frac{\dot{v}}{v} & \delta \end{matrix}]^\top$ and

$$A(p) = \begin{bmatrix} -\frac{\dot{v}}{v} & -1 & \frac{c_f}{mv} & \frac{c_r}{mv} & 0 \\ 0 & 0 & \frac{l_f c_f}{I_{zz}} & -\frac{l_r c_r}{I_{zz}} & 0 \\ -\frac{v}{\sigma} & -\frac{l_f}{\sigma} & -\frac{v}{\sigma} & 0 & \frac{v}{\sigma} \\ -\frac{v}{\sigma} & \frac{l_r}{\sigma} & 0 & -\frac{v}{\sigma} & 0 \\ 0 & 0 & n(\delta)c_f b_l & 0 & -a_\delta \end{bmatrix}, B_b = \begin{bmatrix} 0 \\ 0 \\ 0 \\ 0 \\ b_b \end{bmatrix}. \quad (21)$$

The input of the model is τ_s, while the vehicle speed v and acceleration $a = \dot{v}$ are external scheduling signals and the steering angle δ is both a scheduling and a state variable. Physical parameters of the model are collected in $\theta_{st} \triangleq [c_f\ c_r\ l_r\ I_{zz}\ \sigma\ A\ a\ b\ a_\delta\ b_b\ b_l\ n_1\ \ldots\ n_{11}]^\top$, where $n_i = n(\delta_i)$, $i \in \{1, \ldots, 11\}$, are parameters of a piecewise-linear approximation of $n(\delta)$ over an evenly spaced fixed grid $\{\delta_i\}$ of steering angles. The scheduling set $\mathbb{P} \subset \mathbb{R}^{n_p=3}$ in which p is assumed to take values during operation is considered to be $\mathbb{P} = [2,\ 8]\frac{m}{s} \times [-0.3,\ 0.3]s^{-1} \times [-0.53,\ 0.53]$rad. The yaw-rate output of the model is denoted by $\hat{r}(\theta_{st})$.

3.2 Modeling Approach

The LPV-ST model is discretized via 4$^{\text{th}}$-order RK with $T_s = 0.1$s and its parameters θ_{st} are optimized by *nonlinear least-squares* (NLS) (Coleman and Li, 1996). For this purpose, system model derived in Section 2 was simulated according to the experimental conditions and excitation signals detailed in Section 5. Let $\{r_k\}_{k=0}^N$ be the resulting sampled output sequence of the true system at sampling times kT_s and $\{p_k\}_{k=0}^N$ the corresponding scheduling. As an objective function, the ℓ_2 loss of the model simulation error is considered, giving the optimization problem

$$\min_{\theta_{st}} \sum_{k=1}^N (r_k - \hat{r}_k(\theta_{st}))^2 \text{ subject to } \underline{\theta} \leq \theta_{st} \leq \bar{\theta}, \qquad (22)$$

where $\hat{r}_k(\theta_{st})$ is the simulated LPV-ST model response

under scheduling p_k and parameter values θ_{st}, while $\underline{\theta}$ and $\bar{\theta}$ are predefined bounds. Note that the 4$^{\text{th}}$-order RK is used as it has low local truncation error and can be applied to both nonlinear and LPV models.

4. BLACK-BOX LPV IDENTIFICATION

Compared to approximation and embedding-based LPV modeling of the nonlinear system dynamics, in this section we discuss data-based black-box modeling of the system.

4.1 Model Structures

To identify the data-generating system, we will consider discrete-time LPV *input-output* (IO) models (see Tóth et al. (2012)) of the form

$$\mathcal{F}_\theta(q^{-1}, p_k)\breve{y}_k = \mathcal{B}_\theta(q^{-1}, p_k)q^{-\tau_d}u_k, \quad (23a)$$

$$\mathcal{D}_\theta(q^{-1}, p_k)v_k = \mathcal{C}_\theta(q^{-1}, p_k)\varepsilon_{k|\theta}, \quad (23b)$$

$$\mathcal{A}_\theta(q^{-1}, p_k)y_k = \breve{y}_k + v_k, \quad (23c)$$

where $k \in \mathbb{Z}$ is the discrete time, $y : \mathbb{Z} \to \mathbb{R}$ is the measured output signal, i.e., the measured yaw rate r, $u : \mathbb{Z} \to \mathbb{R}$ denotes the input signal, i.e., the torque τ_s, $p : \mathbb{Z} \to \mathbb{P}$ is the scheduling variable, $\varepsilon_{k|\theta}$ is a noise process (residual error), assumed to be white, and q^{-1} is the backward time-shift operator, i.e., $q^{-1}u_k = u_{k-1}$. The terms $\mathcal{A}_\theta, \dots, \mathcal{F}_\theta$ are polynomials in the time-operator q^{-1} in the form:

$$\mathcal{M}(\xi, p_k) = m_0(p_k) + \sum_{i=1}^{n_m} m_i(p_k)q^{-i}, \quad (24)$$

with coefficient functions

$$m_i(p_k) = \sum_{j=1}^{n_{poly}} \sum_{l=1}^{n_p} m_{i,j,l} \cdot p_{k,i}^j, \quad (25)$$

corresponding static polynomial dependence on $p_k = [p_{k,1} \ p_{k,2} \ p_{k,3}]^\top$ and the parameters $m_{i,j,l} \in \mathbb{R}$ constitute the parameter vector θ associated with the model structure (23). Furthermore, all polynomials are assumed to be monic, i.e., with $m_0(p_k) \equiv 1$ except $\mathcal{B}_\theta$. The model structure (23) with $\mathcal{A} \triangleq I$ is also known as the LPV *Box-Jenkins* (BJ) model. By considering $\mathcal{C} \triangleq \mathcal{D} \triangleq \mathcal{F} \triangleq I$ in (23), the LPV version of the so-called *auto regressive with exogenous input* (ARX) model structure is obtained. Similarly, the *auto regressive moving average with exogenous input* (ARMAX) model is found by considering $\mathcal{D} \triangleq \mathcal{F} \triangleq I$, and the *output-error* (OE) model by $\mathcal{A} \triangleq \mathcal{C} \triangleq \mathcal{D} \triangleq I$. The model structure (23) makes possible to capture both the deterministic dynamics of the steering system in terms of (23a) and the combined effect of the process noise d and measurement noise e in terms of (23b).

4.2 Model Estimation

This section provides a short overview of *prediction-error minimization* (PEM) based estimation of LPV-IO models (23). For a more detailed description, see e.g. Tóth et al. (2012). In PEM, model estimates are obtained by minimizing their associated *one-step-ahead* prediction-error with respect to a loss function where the (unknown) model parameters θ are the optimization variables. A parameter estimate $\hat{\theta}_N$ is obtained by minimizing the least-squares criterion, i.e. the ℓ_2-loss of the prediction error

$$\hat{\theta}_N = \underset{\theta \in \mathbb{R}^{n_\theta}}{\text{argmin}} \ V(\mathcal{D}_N, \theta), \quad (26)$$

with

$$V(\mathcal{D}_N, \theta) = \frac{1}{N} \sum_{k=1}^{N} \|\varepsilon_{k|\theta}\|_2^2 = \frac{1}{N}\|\varepsilon_\theta\|_{\ell_2}^2,$$

where $\mathcal{D}_N = \{u_k, p_k, y_k\}_{t=1}^N$ is the observed data sequence of the system and the one-step-ahead prediction-error is $\varepsilon_{k|\theta} = y_k - \hat{y}_{k|\theta,k-1}$. The exact approach to calculate the predictor $\hat{y}_{k|\theta,k-1}$ based on (23) is discussed in Tóth et al. (2012). In order to calculate model estimates via (26), we use the LPVcore toolbox, see den Boef et al. (2021) that is available at `www.lpvcore.net`. The toolbox contains four time-domain methods for identifying IO model structures (23): 1) linear regression, 2) pseudo-linear regression, 3) gradient-based search, and 4) instrumental variable method. These methods are based on (Laurain et al. (2010); Tóth et al. (2012)). Linear regression is applicable for the ARX model set and can be used with regularization to solve a Tikhonov regression problem, where various weighting matrices can be automatically tuned using generalized cross-validation. Pseudo-linear regression and gradient-based search are available for ARMAX, OE, and BJ models. Initialization of the latter algorithms is provided either by ARX estimation using linear regression or IV-based estimates.

5. EXPERIMENTAL CAMPAIGN

The discrete implementation of the overall system dynamics with inputs τ_s, v, a and noise processes d and e as discussed in Section 2 are used as a data generating system. Two data sets $N = 5000$ samples are collected, one for estimation $\mathcal{D}_N^{id} = \{(\tau_{s,k}^{id}, v_k, a_k, \delta_k^{id}, r_k^{id})\}_{k=0}^N$ with noise (SNR = 12.4dB) and one for model validation $\mathcal{D}_N^{va}$ with different realization of the inputs and with no noise (d and e set to zero). The driving/braking forces are chosen such that a given speed profile is followed; therefore, speed v_k and acceleration a_k are common in both data sets. Given the speed profile, inputs $\tau_{s,k}^{id}$ and $\tau_{s,k}^{va}$ are computed such that for the corresponding boost torques we have two independently generated, normally distributed, zero-mean random sequences with standard deviation 0.3, i.e., $\tau_{b,k}^{id}, \ \tau_{b,k}^{va} \sim \mathcal{N}(0, 0.3^2)$. The chosen speed profile, input torque, the boost map function and the resulting boost torque are illustrated in Figure 2. The effect of noise present in $\mathcal{D}_{id}$ can be observed in Figure 3.

6. IDENTIFICATION RESULTS

LPV-ST model has been developed to provide a simple LPV embedding and approximation of the original dynamics of the system and also to provide construction of the scheduling variable on which the identification via the black box approaches is based on. In case the true physical parameters are substituted in the LPV-ST model, the resulting model performs poorly on the noise-free validation data set $\mathcal{D}_N^{va}$, where its simulated response achieves a best-fit-rate of BFR = 57.3% with

$$\text{BFR} = 100 \cdot \max\left(1 - \frac{\|y - \hat{y}\|_2}{\|y - \bar{y}\|_2}, 0\right) [\%] \quad (27)$$

where $\bar{y}$ is the mean of the reference output y and $\hat{y}$ is the model response. This clearly shows that the involved approximations (e.g., neglecting roll and pitch dynamics) result in a serious approximation error. By using NLS, the parameters of the LPV-ST model are estimated using $\mathcal{D}_N^{id}$ and the results are given in Table 4, while the simulation
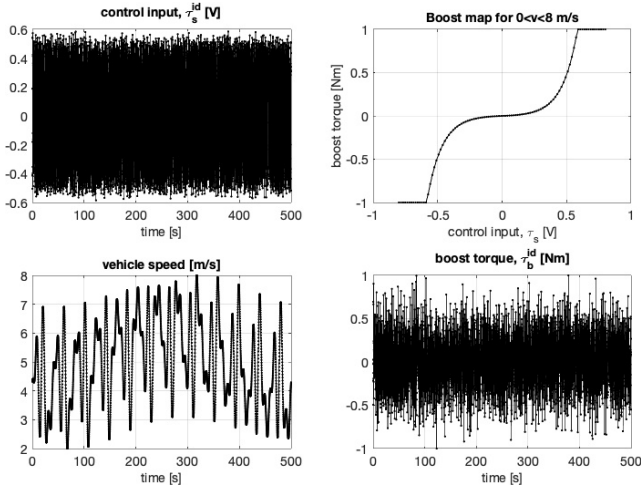
Fig. 2. Input data τ_s^{id} and speed v for the identification data set (left); input nonlinearity (boost map) and the corresponding boost torque τ_b^{id}.
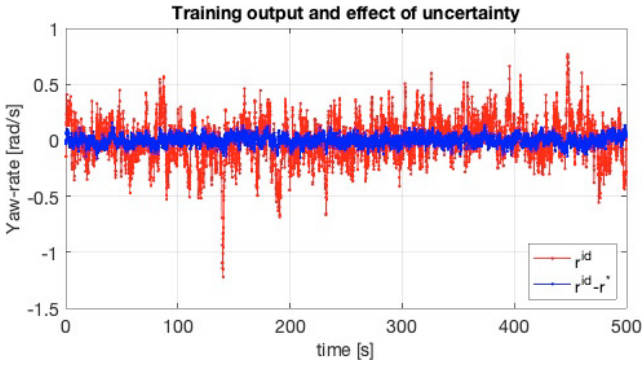

Fig. 3. Contribution (given by blue) of the process noise d and measurement noise e in the measured yaw-rate output r^{id} (given by red) in $\mathcal{D}_N^{id}$.
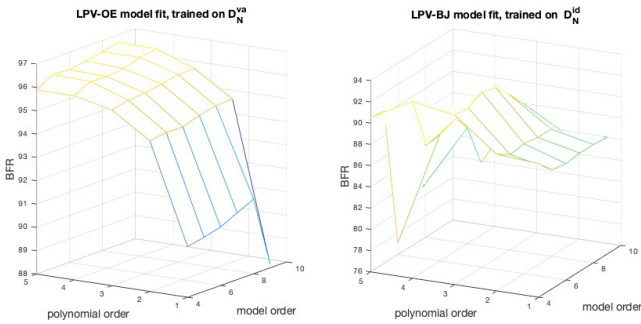

Fig. 4. Model order selection. LPV-OE (left) and LPV-BJ (right) models are identified respectively on the nose-free data set $\mathcal{D}_N^{va}$ and the noisy data set $\mathcal{D}_N^{id}$.

error on the validation set is plotted in Figure 5. We can see that with adjusted parameters, the simplified model dynamics are capable to achieve improved representation of the system which is a well-known phenomenon in model reduction.

Using LPVcore, identification of the steering system based on $\mathcal{D}_N^{id}$ with various model structures in terms of (23) has been carried out. Based on canonical correlation analysis, the delay n_d has been identified to be 1 sample.
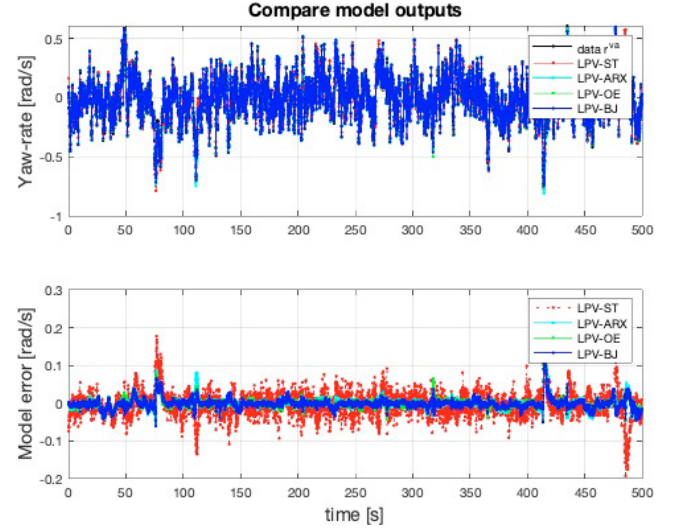

Fig. 5. LPV models identified from noisy data set $\mathcal{D}_N^{id}$ are compared on the nose-free data set $\mathcal{D}_N^{va}$.

Selection of the order [2] of process and noise part has been analyzed both on noise-free (LPV-OE estimation) and noisy data (LPV-BJ estimation). The results are depicted on Figure 4. Based on the noise free results we can see that polynomial dependency of order 3 and 4 can provide effective representation of the process dynamics while polynomial order above 5 has no significant improvement on the representation error. Estimation results in the noisy case reveal that the available length of the data-sequence is not enough for the reliable estimation of LPV-BJ models with high order polynomial dependencies. Based on the results, process and noise model order of 4 with polynomial dependency of order 4 is chosen. The detailed estimation results with various model structures can be seen in Table 4 for this specific case. For the same models, simulation plots on the validation data set $\mathcal{D}_N^{va}$ are shown in Figure 5. It is evident that the ARX model results in a biased estimate in terms of low BFR validation results compared to the high estimation score due to the harsh combination of process and measurement noise present in the system. The OE model is capable to provide an unbiased estimate of the process model while the ARMAX structure is capable to well approximate the noise process and mitigate the bias that was observed in the ARX case, getting close to the validation results of the OE case. The BJ structure is capable to further refine the noise model and even get a better estimate of the process model than OE shown by its improved simulation results. However, the improvement is small, which clearly shows a dominant ARMA nature of the combined noise process. Compared to the ST case, it is apparent that the presented black-box structures are needed to obtain compact LPV models in discrete-time as the approximation and embedding path leads to much worse model fit. Despite the 12 dB SNR, the methods get close to the noise free performance as it can be seen at the bottom of Table 4.

---

[2] Note that order selection is required due to the approximative nature of the LPV model structures with polynomial dependency and the noise induced bias-variance trade-off. Furthermore it is difficult to determine optimal order choice for LPV modeling of the involved noise processes.

Table 4. BFR results of the models with process and noise model order 4, and 4th-order polynomial dependency. Prediction error is computed on set $\mathcal{D}_N^{\mathrm{id}}$, while simulation error is computed on set $\mathcal{D}_N^{\mathrm{va}}$

	ARX	OE	ARMAX	BJ	ST
Identified on noisy $\mathcal{D}_N^{\mathrm{id}}$					
Prediction	83.0%	78.0%	83.02%	82.5%	72.6%
Simulation	71.6%	92.4%	90.81%	92.6%	83.2%
Identified on noisefree $\mathcal{D}_N^{\mathrm{va}}$					
Simulation	93.4%	95.9%	-	-	84.9%

7. CONCLUSIONS

In this paper, we have studied identification of the steering system of a Nissan Leaf based autonomous car using a high-fidelity model as the data-generating system. By comparing parameter-estimation of a single-track approximation based LPV physical model with the result of black-box identification of input-output models we have shown that LPV system identification can deliver efficient model of the process dynamics even under harsh noise conditions. Based on the results of our study, we aim to carry out an experimental camping on the real vehicle and apply the discussed methods together with subspace methods to obtain efficient LPV model of the dynamics for control design. We also aim to involve experiments of higher speed, changing adhesion characteristics and combined braking and steering maneuvers to increase the representation capability and validity range of the obtained model.

REFERENCES

Althoff, M., Koschi, M., and Manzinger, S. (2017). Commonroad: Composable benchmarks for motion planning on roads. In *Proc. of the IEEE Intelligent Vehicles Symposium*, 719–726.

Anderson, J.M., Nidhi, K., Stanley, K.D., Sorensen, P., Samaras, C., and Oluwatola, O.A. (2014). *Autonomous vehicle tech.: A guide for policymakers.* Rand Corp.

Berntorp, K. (2013). Derivation of a six degrees-of-freedom ground-vehicle model for automotive applications. Technical report, Lund University. TFRT-7627.

Berntorp, K., Olofsson, B., Lundahl, K., and Nielsen, L. (2014). Models and methodology for optimal trajectory generation in safety-critical road-vehicle manoeuvres. *Vehicle System Dynamics*, 52(10), 1304–1332.

Bertolazzi, E., Biral, F., and Lio, M.D. (2007). Real-time motion planning for multibody systems. *Multibody System Dynamics*, 17(2), 119–139.

Coleman, T. and Li, Y. (1996). An interior, trust region approach for nonlinear minimization subject to bounds. *SIAM Journal on Optimization*, 6, 418–445.

Cox, P.B. and Tóth, R. (2021). Linear parameter-varying subspace identification: A unified framework. *Automatica*, 123, 109296.

den Boef, P., Cox, P.B., and Tóth, R. (2021). LPVcore: MATLAB toolbox for LPV modelling, identification and control of non-linear systems. In *Proc. of the 19th IFAC Symposium System Identification.* Padova, Italy.

Hjartarson, A., Seiler, P., and Packard, A. (2015). LPV-Tools: A toolbox for modeling, analysis, and synthesis of parameter varying control systems. In *Proc. of the 1st IFAC Workshop on Linear Parameter Varying Systems*, 139–145. Grenoble, France.

Hoffmann, C. and Werner, H. (2015). A survey of linear parameter-varying control applications validated by experiments or high-fidelity simulations. *IEEE Trans. Control Systems Technology*, 23(2), 416–433.

Kiencke, U. and Nielsen, L. (2000). *Automotive control systems for engine, driveline and vehicle.* Springer.

Laurain, V., Gilson, M., Tóth, R., and Garnier, H. (2010). Refined instrumental variable methods for identification of LPV Box-Jenkins models. *Automatica*, 46(6), 959–967.

Ljung, L. (1999). *System Identification, theory for the user.* Prentice-Hall, 2nd edition.

Poussot-Vassal, C., Sename, O., Fergani, S., Doumiati, M., and Dugard, L. (2013). Global chassis control using coordinated control of braking/steering actuators. In O. Sename, P. Gaspar, and J. Bokor (eds.), *Robust Control and Linear Parameter Varying Approaches*, 237–265. Springer.

Rödönyi, G., Beintema, G., Tóth, R., Schoukens, M., Pup, D., Kisari, Á., Vígh, Z., Kőrös, P., Soumelidis, A., and Bokor, J. (2021). Identification of the nonlinear steering dynamics of an autonomous vehicle. In *Proc. of the 19th IFAC Symposium on System Identification.* Padova, Italy.

Schoukens, J. and Ljung, L. (2019). Nonlinear system identification: A user-oriented road map. *IEEE Control Systems Magazine*, 39(6), 28–99.

Singh, K.B. and Taheri, S. (2015). Estimation of tire-road friction coefficient and its application in chassis control systems. *Systems Science & Control Eng.*, 3(1), 39–61.

Szűcs, B., Kisari, Á., Kőrös, P., Pup, D., Rödönyi, G., Soumelidis, A., and Bokor, J. (2020). Experimental verification of a control system for autonomous navigation. In *Proc. of the IFAC World Congress.* Berlin, Germany.

Tóth, R. (2010). *Modeling and Identification of Linear Parameter-Varying Systems.* Lecture Notes in Control and Information Sciences, Vol. 403. Springer.

Tóth, R., Heuberger, P.S.C., and Van den Hof, P.M.J. (2012). Pediction error identification of LPV systems: present and beyond. In J. Mohammadpour and C.W. Scherer (eds.), *Control of Linear Parameter Varying Systems with Applications*, 27–60. Springer.